Cell

Genetic Tracing via DNGR-1 Expression History Defines Dendritic Cells as a Hematopoietic Lineage

Barbara U. Schraml,[1] Janneke van Blijswijk,[1] Santiago Zelenay,[1] Paul G. Whitney,[1] Andrew Filby,[2] Sophie E. Acton,[1,3] Neil C. Rogers,[1] Natalia Moncaut,[4] Jaime J. Carvajal,[4,5] and Caetano Reis e Sousa[1,*]
[1]Immunobiology Laboratory
[2]Flow Cytometry Laboratory
Cancer Research UK, London Research Institute, Lincoln's Inn Fields Laboratories, 44 Lincoln's Inn Fields, London WC2A 3LY, UK
[3]Department of Cell and Developmental Biology, University College London, London WC1E 6BT, UK
[4]Division of Cancer Biology, The Institute of Cancer Research, Chester Beatty Laboratories, 237 Fulham Road, London SW3 6JB, UK
[5]Centro Andaluz de Biología del Desarrollo, CSIC-UPO-JA, Sevilla 41013, Spain
*Correspondence: caetano@cancer.org.uk
http://dx.doi.org/10.1016/j.cell.2013.07.014

SUMMARY

Mononuclear phagocytes are classified as macrophages or dendritic cells (DCs) based on cell morphology, phenotype, or select functional properties. However, these attributes are not absolute and often overlap, leading to difficulties in cell-type identification. To circumvent this issue, we describe a mouse model to define DCs based on their ontogenetic descendence from a committed precursor. We show that precursors of mouse conventional DCs, but not other leukocytes, are marked by expression of DNGR-1. Genetic tracing of DNGR-1 expression history specifically marks cells traditionally ascribed to the DC lineage, and this restriction is maintained after inflammation. Notably, in some tissues, cells previously thought to be monocytes/macrophages are in fact descendants from DC precursors. These studies provide an in vivo model for fate mapping of DCs, distinguishing them from other leukocyte lineages, and thus help to unravel the functional complexity of the mononuclear phagocyte system.

INTRODUCTION

Dendritic cells (DCs) play a key role in immune regulation. Historically, DCs have been identified as nonlymphocytic motile cells of dendritic morphology, expressing high levels of major histocompatibility complex class II molecules (MHCII) and the integrin CD11c (Geissmann et al., 2010; Hashimoto et al., 2011; Heath and Carbone, 2009; Steinman and Idoyaga, 2010). In addition, functional criteria, including migratory capacity and superior ability to stimulate T lymphocytes, are often used to distinguish DCs from other mononuclear phagocytes such as macrophages (MØs) and monocytes (Hashimoto et al., 2011; Milling et al., 2010; Steinman and Idoyaga, 2010). However, functional attributes are not discrete cellular properties, and phenotypic markers are often shared among related cell types, particularly after infection or during inflammation when they are up- and downregulated. The inability to accurately distinguish DCs and MØs has led to confusion and debate and makes it difficult to assess whether individual mononuclear phagocyte subtypes have unique functions in the immune system (Hashimoto et al., 2011; Hume, 2008).

Gene expression analysis and ontogenetic relationships have been used to refine the definition of DCs and MØs. For instance, two types of MØs and two subsets of DCs have been described across lymphoid and nonlymphoid tissues of both mice and humans by comparing gene expression signatures and/or demonstrating that the development of a given population depends on a specific transcription factor, cytokine, or growth factor (Gautier et al., 2012; Geissmann et al., 2010; Greter et al., 2012; Haniffa et al., 2012; Hashimoto et al., 2011; Heath and Carbone, 2009; Hildner et al., 2008; Meredith et al., 2012a; Miller et al., 2012; Persson et al., 2013; Satpathy et al., 2012; Satpathy et al., 2011; Schlitzer et al., 2013; Schulz et al., 2012; Tussiwand et al., 2012). Nevertheless, there remains the need for an overarching ontogenetic definition that unifies the DC family and establishes it as an independent leukocyte lineage (Hashimoto et al., 2011).

Mouse bone marrow (BM) cells lacking lineage-restricted markers (lin) and expressing CD115 (M-CSF receptor), CD135 (fms-like tyrosine kinase receptor-3), CX_3CR1, and low levels of CD117 (c-kit, stem cell factor receptor) give rise only to DCs after in vitro culture or transfer into mice and are termed common DC precursors (CDPs) (Auffray et al., 2009; Liu et al., 2009; Naik et al., 2007; Onai et al., 2007). CDPs do not exit the BM but give rise to pre-DCs, which migrate through the blood to lymphoid and nonlymphoid organs, where they terminally differentiate into conventional DCs (cDCs), including the two main $CD11b^+$ and $CD11b^-$ cDC subsets (Ginhoux et al., 2009; Liu et al., 2009; Naik et al., 2006, 2007; Onai et al., 2007). In contrast, plasmacytoid DCs (pDCs) are thought to derive from CDPs

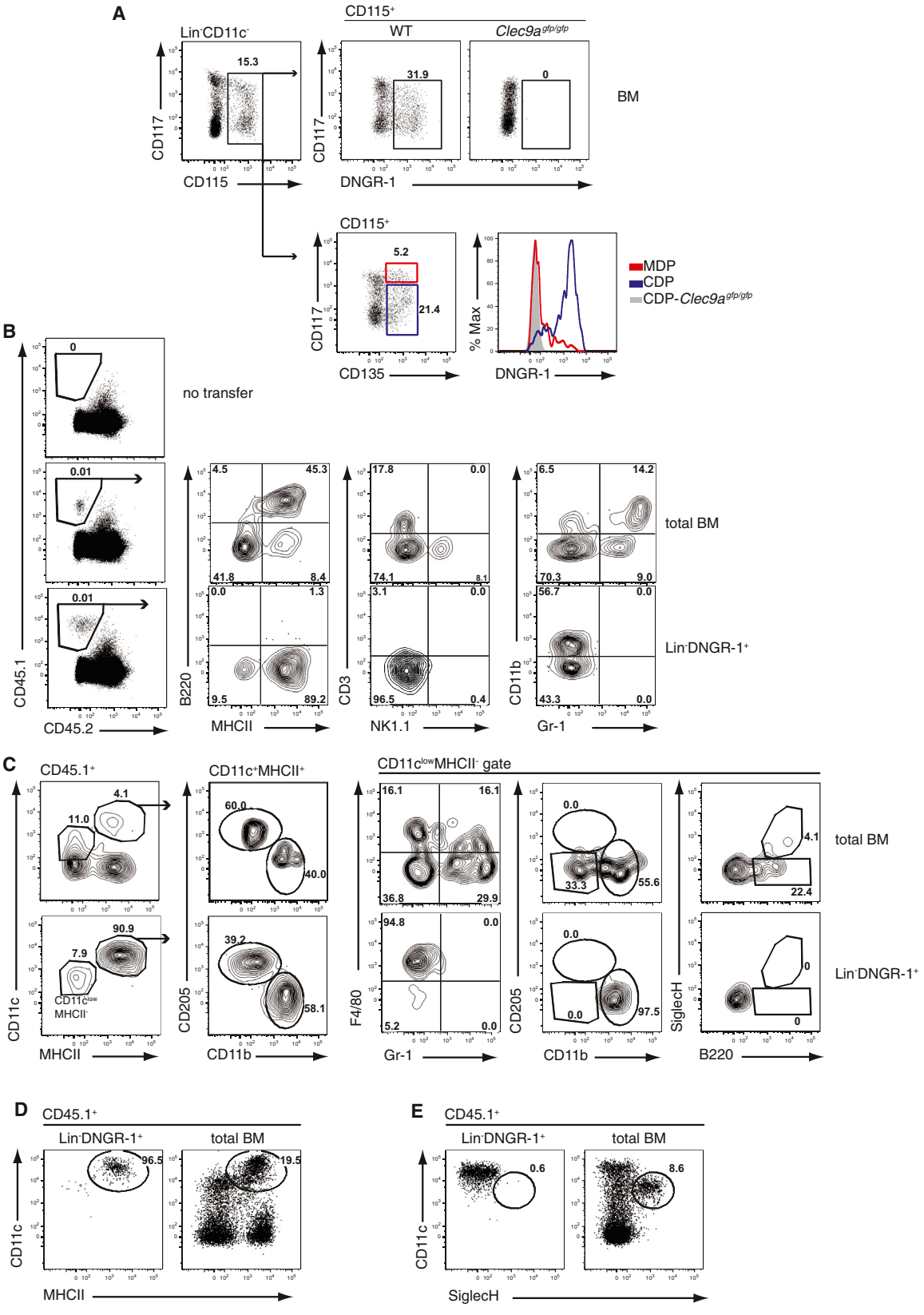

(legend on next page)

independently of pre-DCs (Liu et al., 2009; Naik et al., 2007; Onai et al., 2007), although their CDP origin has recently been questioned (Onai et al., 2013).

As ontogeny is immutable, the tracking of CDP and pre-DC progeny should allow for definition of the DC lineage irrespective of markers or functional criteria. This would help resolve issues of nomenclature within the mononuclear phagocyte family and provide a system for studying DC dynamics in the steady state and after inflammation or infection. Here, we report that precursors of cDC can be defined in mice by expression of the C-type lectin receptor DNGR-1 and describe a model for genetic labeling of DNGR-1-expressing cells and their progeny that allows for ontogenetic definition of the DC lineage in mice.

RESULTS

DNGR-1 Marks CDP and Pre-DC

DNGR-1 (also known as CLEC9A) is expressed at high levels by CD8α^+ and CD103$^+$CD11b$^-$ cDCs and at lower levels by pDCs in mice (Caminschi et al., 2008; Poulin et al., 2012; Sancho et al., 2008). We additionally noticed the presence of low levels of the receptor on splenic pre-DCs, defined as lin$^-$ CD11c$^+$CD43$^+$ CD135$^+$CD172a^{low} cells (Naik et al., 2006), from wild-type, but not control DNGR-1-deficient (*Clec9a*$^{gfp/gfp}$) mice (Sancho et al., 2009; Figure S1A available online). Pre-DCs from BM also expressed DNGR-1 (Figure S1B). In that organ, DNGR-1$^+$ cells were additionally found in the lin$^-$CD11c$^-$CD115$^+$ compartment, which includes MØ/DC precursors (MDPs; Fogg et al., 2006) and CDPs (Figure 1A). However, DNGR-1 expression correlated with lower levels of CD117 (Figure 1A), a phenotype associated with CDP activity in transfer studies (Auffray et al., 2009; Naik et al., 2007; Onai et al., 2007). Indeed, we found unimodal DNGR-1 expression on CD117^{low}, but not on CD117^{hi} cells or on CD117^{low} cells from control *Clec9a*$^{gfp/gfp}$ BM (Sancho et al., 2009) (Figures 1A and S1C). The lin$^-$CD11c$^-$DNGR-1$^+$ cells additionally expressed CD135, but not CD127 (IL-7Rα), a marker for lymphoid precursors (Schlenner et al., 2010) (data not shown), and therefore phenotypically resembled CDPs.

To establish that DNGR-1 marks progenitors with DC-restricted potential, we sorted lin$^-$CD115$^+$DNGR-1$^+$ cells from BM of CD45.1 B6.SJL mice irrespective of CD117 levels (Figure S1D; called lin$^-$DNGR-1$^+$ cells) and transferred them into unirradiated CD45.2 congenic hosts. Control (unfractionated) BM gave rise to a variety of lymphoid and myeloid lineages, including B (B220$^+$MHCII$^+$), T (CD3$^+$), and NK (NK1.1$^+$CD3$^-$) cells, neutrophils/monocytes (Gr-1$^+$CD11b$^+$), and cDCs (CD11c$^+$MHCII$^+$) (Figures 1B and 1C). In contrast, lin$^-$DNGR-1$^+$ cells generated almost exclusively CD11c$^+$MHCII$^+$ cDCs, including both CD11b$^-$ (also known as CD8α^+, identified here by CD205 expression) and CD11b$^+$ subsets at the expected ratio (Figures 1B and 1C; data not shown).

The progeny of lin$^-$DNGR-1$^+$ cells also included CD11c^{low}MHCII$^-$ cells. These cells lacked the pDC markers Gr-1, B220, or SiglecH, in contrast to CD11c^{low}MHCII$^-$ cells derived from total BM (Figure 1C), but expressed low levels of F4/80 and CD11b (Figure 1C), suggesting that they might constitute pre-DCs (Naik et al., 2006). Consistent with that notion, lin$^-$DNGR-1$^+$ BM cells gave rise exclusively to CD11c$^+$MHCII$^+$ cDCs after transfer into sublethally irradiated hosts, where an increased niche favors terminal differentiation of the donor cells (Figure 1D). In contrast, control total BM gave rise to multiple cell types, including pDCs (Figures 1D and 1E). Thus, in adoptive transfers, lin$^-$DNGR-1$^+$ cells specifically give rise to cDCs, but not pDCs or other lymphoid or myeloid cells, indicating that DNGR-1 marks cDC-restricted precursors. We continue to refer to the DNGR-1$^+$CD11c$^-$ precursor as "CDP" even though our data would suggest that the acronym is better expanded as "conventional DC precursor" (see Discussion).

Clec9a-Cre Mice Allow Genetic Marking of CDP in BM and Their Progeny in Lymphoid Tissues

We hypothesized that tracing the expression history of DNGR-1 would allow us to determine the ontogenetic contribution of CDPs and pre-DCs to the mononuclear phagocyte system. We generated mice expressing Cre recombinase under control of the *Clec9a* locus by homologous recombination (Figures S2A and S2B) and crossed them to Rosa26-stop^{flox}-enhanced yellow fluorescent protein (YFP) reporter mice (Srinivas et al., 2001) (hereafter referred to as *Clec9a*$^{+/+}$*Rosa*$^{+/EYFP}$ or *Clec9a*$^{+/cre}$*Rosa*$^{+/EYFP}$ mice, indicating the genotype at both loci). In *Clec9a*$^{+/cre}$*Rosa*$^{+/EYFP}$ mice, Cre-mediated excision of a floxed stop codon is predicted to lead to constitutive expression of YFP, thus irreversibly marking DNGR-1-expressing cells and their progeny.

We first validated that *Clec9a*-driven Cre is active in DC precursors. Indeed, YFP was detected in CDPs and pre-DCs, but not MDPs of *Clec9a*$^{+/cre}$*Rosa*$^{+/EYFP}$ mice, as defined phenotypically (Figures 2A–2C). However, only a fraction of the DC precursors was labeled, indicating that recombination of the stop codon at the population level is incomplete (see below). Nevertheless, we found YFP$^+$ cells in spleen of *Clec9a*$^{+/cre}$*Rosa*$^{+/EYFP}$, but not *Clec9a*$^{+/+}$*Rosa*$^{+/EYFP}$ mice (Figures 2D–2F). The majority of YFP$^+$ splenocytes were

Figure 1. DNGR-1 Marks Cells with cDC Restricted Differentiation Potential

(A) Lin$^-$ (Ter119, NK1.1, CD4, CD8, B220, CD11b, and MHCII), CD11c$^-$ BM cells from WT, and *Clec9a*$^{gfp/gfp}$ mice were analyzed for CD117, CD115, and DNGR-1 by flow cytometry. Top: DNGR-1 and CD117 expression on lin$^-$CD11c$^-$CD115$^+$ cells. Bottom: DNGR-1 expression on lin$^-$CD11c$^-$CD115$^+$ MDP (CD117^{hi}CD135$^+$) and CDP (CD117^{low}CD135$^+$).

(B and C) Lin$^-$CD115$^+$DNGR-1$^+$ cells (lin$^-$DNGR-1$^+$) or total BM from CD45.1 B6.SJL mice were transferred into unirradiated CD45.2 recipients. On day 7, CD45.1$^+$ donor-derived splenocytes were analyzed for expression of lineage markers (B). (C) CD45.1$^+$CD11c$^+$MHCII$^+$ cDCs were analyzed for CD205 and CD11b to identify CD205$^+$CD11b$^-$ DCs and CD11b$^+$CD205$^-$ DCs. CD11c^{low}MHCII$^-$CD45.1$^+$ cells were analyzed for lineage markers. Data are representative of three experiments with two to three mice per group.

(D and E) CD45.1$^+$ lin$^-$CD115$^+$DNGR-1$^+$ (lin$^-$DNGR-1$^+$, n = 5) or total BM (n = 6) cells were transferred into sublethally irradiated CD45.2 recipients. On day 7, splenic CD45.1$^+$ cells were analyzed for CD11c and MHCII (D) or CD11c and SiglecH (E) expression.

See Figure S1.

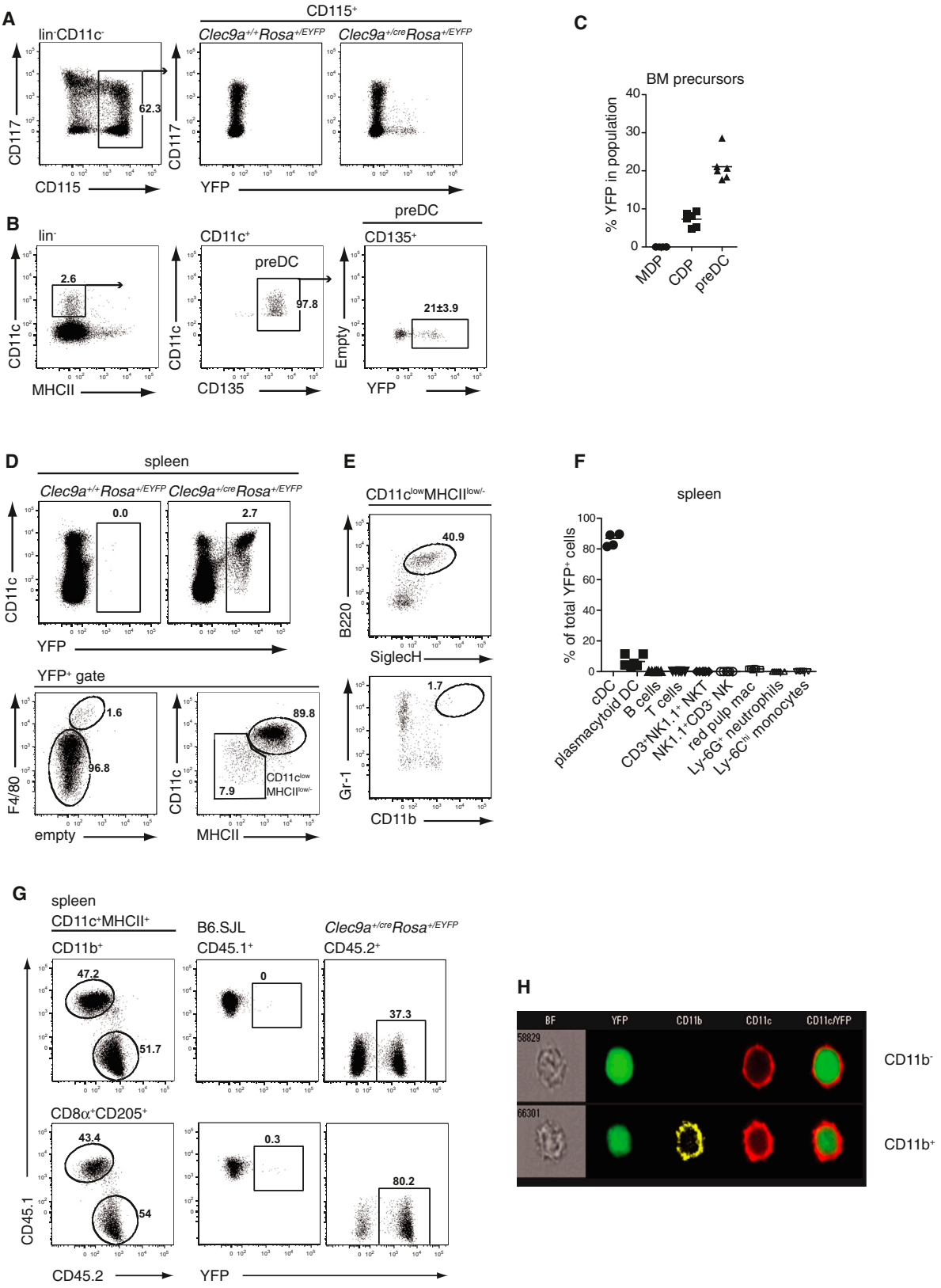

(legend on next page)

CD11c$^+$MHCII$^+$ cDCs (86.9% ± 4%), whereas a minor fraction (1.7% ± 0.4%) resembled F4/80^{hi} autofluorescent red pulp MØs. The remainder was CD11c^{low}MHCII$^{low/-}$ and included cells expressing SiglecH, B220, and Gr-1, but not CD11b, which resembled pDCs (Figures 2D and 2E). The YFP signal was cell autonomous and did not result from bystander uptake of YFP$^+$ cells or cell debris as determined by the use of mixed BM chimeras (Figure 2G). This was additionally supported by image analysis showing uniform cytosolic rather than endosomal localization of YFP (Figure 2H). Systematic analysis of YFP$^+$ splenocytes revealed minimal contribution of B, T, NK, and NKT cells, neutrophils, or Ly-6C^{hi} monocytes (Figures 2F, S2C, and S2D). No YFP labeling of erythrocytes or nonhematopoietic cells was observed (data not shown).

We next assessed the presence and penetrance of the YFP signal in spleen DC subpopulations. We found that 99.1% ± 0.4% of CD8α^+ cDCs were YFP$^+$ (Figures 3A and 3B). This high labeling efficiency is to be expected from additive effects of Cre activity in DC precursors and in differentiated CD8α^+ cDCs, which express high levels of DNGR-1 (Caminschi et al., 2008; Sancho et al., 2009). CD11b$^+$ cDCs lack DNGR-1 protein or messenger RNA (mRNA) (Caminschi et al., 2008; Sancho et al., 2009) (Figures 3A, 5E, S4B, and S4C), and any YFP labeling must therefore have occurred during their development. Accordingly, 50% ± 5.2% of CD11b$^+$ cDCs were YFP labeled (Figures 3A and 3B), which is consistent with the incomplete penetrance of Cre-mediated DNA recombination in CDPs and pre-DCs (see Figures 2A–2C). Among CD11b$^+$ spleen cDCs, ESAM^{hi} and ESAM^{low}CD11b$^+$ subsets labeled equally (Figures S3B and S3C), suggesting that both can be generated from CDP in the steady state despite earlier suggestions to the contrary (Lewis et al., 2011).

Interestingly, pDCs showed a much lower degree of YFP labeling (20.6% ± 7.4%) than CD11b$^+$ cDCs (Figures 3A and 3B) even though they express low levels of DNGR-1 (Sancho et al., 2008). This is consistent with our transfer data indicating that pDCs do not descend from DNGR-1$^+$ precursors (see Figures 1C and 1E) and, therefore, do not have the opportunity to excise the stop codon preceding YFP during development. A DC that lacks CD205 expression but expresses CD8α and CX_3CR1 and resembles pDCs has recently been identified (Bar-On et al., 2010; Edelson et al., 2010). Interestingly, 78% ± 5% of these CD8α^+CD205$^-$ plasmacytoid-like DCs (CD8α^+CD205$^-$ pDCs) were labeled with YFP (Figures 3A and 3B) even though they express DNGR-1 at levels comparable to classical pDCs (data not shown; Figure 3A). This high degree of YFP labeling suggests that some CD8α^+CD205$^-$ pDCs may arise from CDP (see Discussion). YFP$^+$ cells were located in the T cell areas of the white pulp, as well as scattered around the red pulp, mimicking the known distribution of DCs in steady state (Figure 3C). Importantly, no YFP signal was observed in CD169$^+$ metallophilic MØs (Figure 3C) or in blood Ly-6C^{hi} and Ly-6C^{low} monocytes, which arise from MDP and can act as precursors of tissue MØs (Figure S3A).

We obtained analogous results when analyzing YFP expression in CD11c$^+$MHCII$^+$ resident cDCs in skin-draining lymph nodes (sdLN; Figures 3D and 3E). In sdLN, we also examined YFP labeling among the CD11c$^+$MHCII^{hi} migratory DCs (Figures 3D and 3E). CD103$^+$ migratory cDCs displayed extensive YFP labeling (91.5% ± 1.4%; Figures 3D and 3E), which is in line with the fact that they express high levels of DNGR-1 (Poulin et al., 2012). CD103$^-$CD207$^-$CD11b$^+$ cells lack DNGR-1 expression (Poulin et al., 2012) but also labeled with YFP (41.2% ± 5%; Figures 3D and 3E), confirming their CDP origin (Ginhoux et al., 2009). Importantly, CD103$^-$CD207$^+$ Langerhans cells (LCs), which predominantly arise from embryonic precursors (Chorro et al., 2009; Hoeffel et al., 2012), showed little YFP expression (2.7% ± 1.1%; Figures 3D and 3E). We obtained equivalent results in spleen and sdLN of Rosa26-stop^{flox}-YFP mice crossed to *Clec9a*-Cre mice generated using a bacterial artificial chromosome (BAC) transgenic approach (Figures S3D–S3F). In sum, tracing the expression history of DNGR-1 reveals CDP-derived populations in lymphoid organs and confirms the cDC-restricted potential of DNGR-1$^+$ precursors.

The incomplete labeling of differentiated DC populations is most likely a direct consequence of incomplete labeling of BM precursors in *Clec9a*$^{+/cre}$*Rosa*$^{+/EYFP}$ and *Clec9a*-Cre BAC x *Rosa*$^{+/EYFP}$ mice (Figure 2C; data not shown). To test this explicitly, we transferred YFP$^-$lin$^-$DNGR-1$^+$ cells from CD45.2 *Clec9a*-Cre BAC x *Rosa*$^{+/EYFP}$ mice into sublethally irradiated CD45.1 congenic hosts. YFP$^-$lin$^-$DNGR-1$^+$ cells exclusively generated cDCs in spleen, including both CD8α^+ and CD11b$^+$ cDCs at the expected ratio (Figure S3G). Importantly and consistent with a time lag between Cre expression and DNA recombination (see Discussion), some YFP$^-$lin$^-$DNGR-1$^+$ CDPs also generated YFP$^+$ cells (Figure S3G). Thus, the incomplete labeling of DC precursors in *Clec9a*-Cre mice is stochastic and not attributable to qualitative differences between YFP$^+$ and YFP$^-$ precursors, supporting the suitability of the genetic model to trace CDP-derived cells.

Figure 2. *Clec9a*$^{+/cre}$*Rosa*$^{+/EYFP}$ Mice Exhibit DC-Restricted YFP Expression

(A–C) Flow cytometry of BM from *Clec9a*$^{+/+}$*Rosa*$^{+/EYFP}$ and *Clec9a*$^{+/cre}$*Rosa*$^{+/EYFP}$ mice. YFP expression on lin$^-$CD11c$^-$CD115$^+$ cells (A) and pre-DCs (lin$^-$CD11c$^+$CD135$^+$, mean percentage ± SD, n = 6) (B) is shown. YFP$^+$ gates were set on cells from *Clec9a*$^{+/+}$*Rosa*$^{+/EYFP}$ control mice (not shown). (C) Percentage of YFP$^+$ cells in MDPs (lin$^-$CD11c$^-$CD115$^+$ CD135$^+$CD117^{hi}), CDPs (lin$^-$CD11c$^-$CD115$^+$CD135$^+$CD117^{low}, see Figure 1A) and pre-DCs (lin$^-$CD11c$^+$CD135$^+$) of *Clec9a*$^{+/cre}$*Rosa*$^{+/EYFP}$ mice.

(D–F) Flow cytometric analysis of spleen from *Clec9a*$^{+/cre}$*Rosa*$^{+/EYFP}$ and *Clec9a*$^{+/+}$*Rosa*$^{+/EYFP}$ mice. (D) Live YFP$^+$ cells were identified and analyzed for the presence of F4/80^{hi} autofluorescent (auto) red pulp MØs and CD11c$^+$MHCII$^+$ cDCs. (E) YFP$^+$CD11c^{low}MHCII$^{low/-}$ cells identified in (D) were further analyzed for Gr-1, SiglecH, and B220. (F) Percentage of the indicated populations out of total YFP$^+$ cells. (C and F) Horizontal bars are the mean from at least two experiments. (G and H) Lethally irradiated mice were injected i.v. with a 1:1 mixture of CD45.1$^+$ B6.SJL and CD45.2$^+$ *Clec9a*$^{+/cre}$*Rosa*$^{+/EYFP}$ BM. CD11b$^+$ and CD8α^+CD205$^+$ splenic CD11c$^+$MHCII$^+$ cDCs were analyzed for donor BM contribution and YFP expression 6–8 weeks later. (H) Representative images from Image Stream, showing YFP signal in CD11c$^+$CD11b$^+$ and CD11c$^+$CD11b$^-$ splenic DCs from *Clec9a*$^{+/cre}$*Rosa*$^{+/EYFP}$ mice. Bright-field images show dendritic cell morphology (60× magnification).

See also Figure S2.

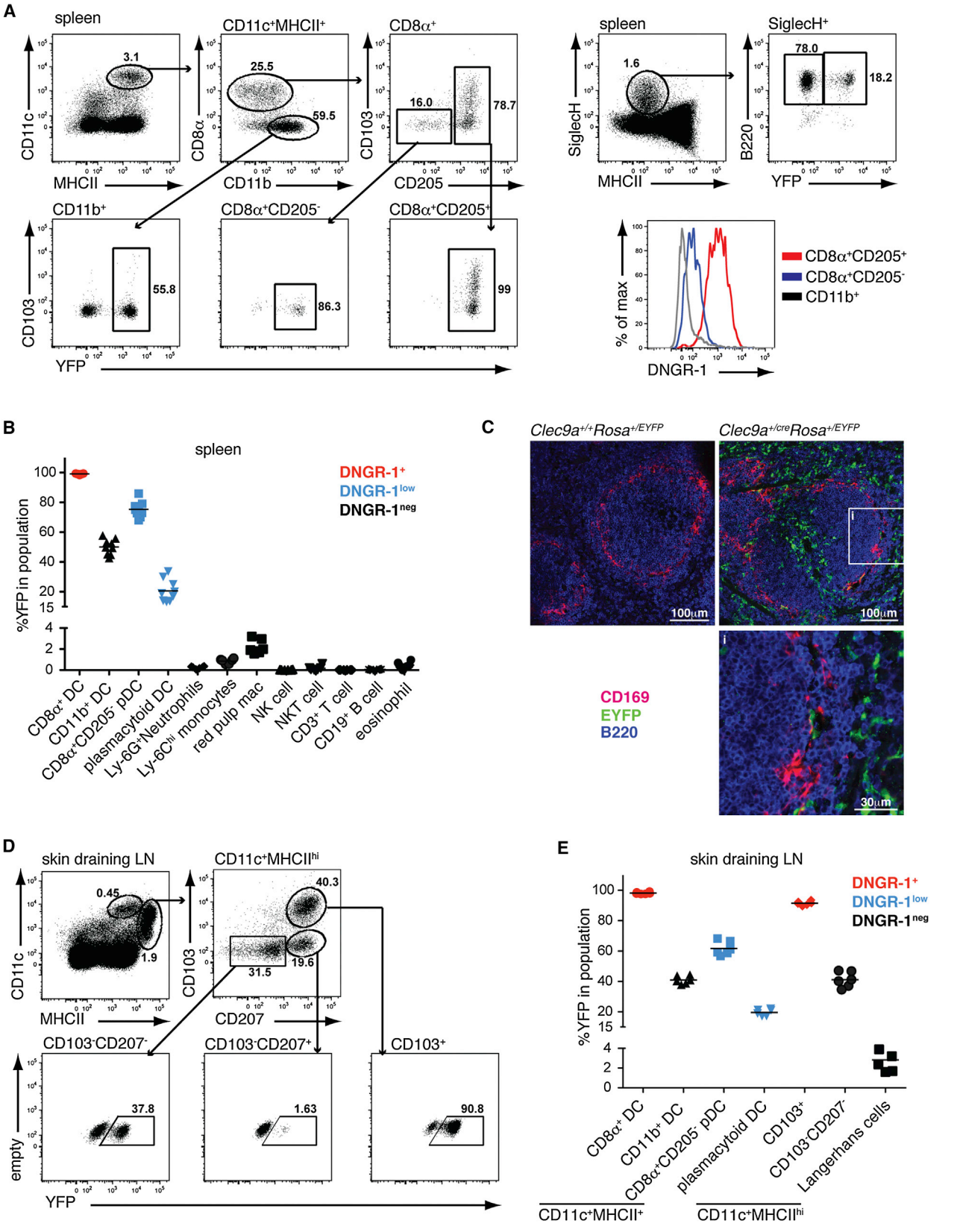

(legend on next page)

Lineage Tracing of CDP-Derived Cells in Nonlymphoid Tissues Reveals Expected and Unexpected Heterogeneity of Mononuclear Phagocytes

We additionally analyzed YFP expression in nonlymphoid tissues. In all tissues examined, there was no labeling of nonhematopoietic CD45$^-$ cells (data not shown). YFP$^+$CD45$^+$ cells were found in lungs of *Clec9a*$^{+/cre}$*Rosa*$^{+/EYFP}$ mice, but not in *Clec9a*$^{+/+}$*Rosa*$^{+/EYFP}$ controls, with cDCs and pDCs accounting for >95% of all YFP$^+$ cells (Figure 4A). To assess labeling of pulmonary DCs, we gated on CD11c$^+$MHCII$^+$ cells (Figure 4C) after excluding CD11c^{hi} autofluorescent alveolar MØs, which are YFP negative (Figure 4B). Within this gate, CD64$^+$CD11b$^+$ cells (Figure 4C) have been argued to represent monocyte progeny (Gautier et al., 2012; Langlet et al., 2012; Plantinga et al., 2013; Tamoutounour et al., 2012). Consistent with that notion, CD64$^+$CD11c$^+$MHCII$^+$ cells were inefficiently labeled with YFP (5.3% ± 1%; Figures 4C and 4D). Among CD11c$^+$MHCII$^+$CD64$^-$ cells, there was near-complete labeling of CD103$^+$ cDCs (97% ± 0.6%; Figures 4C and 4D), which express DNGR-1 (Desch et al., 2011; Poulin et al., 2012), and a lower degree of labeling of CD103$^-$CD11b$^-$ and CD11b$^+$ cells (52% ± 8.4% and 27.6% ± 2.6%, respectively; Figures 4C and 4D), which lack DNGR-1 expression (Poulin et al., 2012). As in lymphoid organs, pDCs were inefficiently labeled (10.3% ± 3.3%, Figure 4D), despite expressing DNGR-1 at low levels. We obtained analogous lineage-tracing results in lungs from *Clec9a*-Cre BAC mice (Figure S4A). In either mouse model, we found no YFP labeling of eosinophils, neutrophils, alveolar MØs, or Ly-6C^{hi} monocytes (Figures 4D and S4A).

In small intestine, CD11c$^+$MHCII$^+$ cells include CD64$^+$ cells marked by intermediate to low levels of CD11c (Figure 4E) and high levels of CD11b (data not shown). These cells likely correspond to monocyte-derived CD11c^{low}CX$_3$CR1$^+$ cells (Bogunovic et al., 2009; Tamoutounour et al., 2012; Varol et al., 2009) and, accordingly, labeled poorly with YFP (6.5% ± 0.9%; Figures 4E and 4F). The CD64$^-$ population could be subdivided into CD103$^+$CD11b$^-$, CD103$^+$CD11b$^+$, and CD103$^-$CD11b$^+$ cells (Figure 4E), as described (Bogunovic et al., 2009). CD103$^+$CD11b$^-$ cDCs express DNGR-1 (Figure S4B and S4C) and labeled extensively with YFP (96% ± 0.8%; Figures 4E and 4F). CD11b$^+$ cells lack DNGR-1 protein and mRNA (Figure S4B and S4C) but labeled strongly with YFP irrespective of CD103 expression (Figures 4E and 4F), suggesting that CD103$^+$CD11b$^+$, as well as CD103$^-$CD11b$^+$ cells, can descend from CDPs.

In kidney, YFP expression encompassed MHCII$^+$ cells with a wide range of CD11c expression (Figure 5A). Therefore, we gated on MHCII$^+$CD45$^+$ cells independently of CD11c levels and divided them into CD64$^+$ and CD64$^-$ populations (Figure 5B). MHCII$^+$CD64$^-$ kidney cells expressed higher levels of CD11c than CD64$^+$ cells and comprised CD103$^+$CD11b$^-$ and CD103$^-$CD11b$^+$ subsets, as well as CD103$^-$CD11b$^-$ cells (Figure 5B). CD103$^+$CD11b$^-$ cDCs express DNGR-1 (Poulin et al., 2012) (Figures 5E and S5A) and labeled extensively with YFP (95% ± 3.5%; Figures 5B and 5C). CD11b$^+$ cells lack DNGR-1 protein or mRNA (Figures 5E and S5A) but were also YFP labeled (33% ± 6.2%; Figures 5B and 5C). Notably, CD103$^-$CD11b$^-$ cells labeled with YFP more efficiently than CD11b$^+$ cells (76% ± 8%; Figures 5B, 5C, and S5B). Thus, most CD11c$^+$CD64$^-$MHCII$^+$ kidney leukocytes are CDP derived, as expected. Surprisingly, MHCII$^+$CD64$^+$ cells in kidney labeled with YFP at frequencies similar to CD64$^-$CD11b$^+$ DCs (29.5% ± 3.7%; Figures 5B, 5C, and S5B). Most kidney CD64$^+$ cells expressed low levels of CD11b and stained strongly for F4/80, unlike in other organs (Figure 5F; see CD45.2$^+$ host cells). Both CD11b^{low} and CD11b^{hi} subpopulations labeled with YFP (Figure 5D) even though they lacked DNGR-1 protein or mRNA (Figures 5E and S5A). These data suggest that, in kidney, CD64 expression does not differentiate CDP-derived from monocyte-derived cells.

We confirmed the CDP origin of CD64$^+$ kidney cells by adoptive transfer of lin$^-$DNGR-1$^+$ BM cells (Figure 5F). In these experiments, most donor-derived CD64$^+$ kidney cells were CD11b^{hi}F4/80^{int} rather than CD11b^{low}F4/80^{hi}, even in control mice receiving total BM (Figure 5F). CD64$^+$CD11b^{low}F4/80^{hi} cells resemble tissue-resident MØs thought to arise from yolk sac progenitors (Schulz et al., 2012). To confirm the BM origin of all kidney YFP$^+$ cells, including the CD64$^+$CD11b^{low} cells, we analyzed BM chimeric mice (Figures 2G, S5C, and S5D). 6 to 8 weeks after reconstitution, CD64$^+$ cells in the kidney contained both CD11b^{hi} and CD11b^{low} populations and, when derived from *Clec9a*$^{+/cre}$*Rosa*$^{+/EYFP}$ donors, labeled with YFP at a frequency comparable to that of CD11b$^+$CD64$^-$ cells (Figures S5C and S5D). Therefore, the underrepresentation of CD11b^{low}F4/80^{hi} cells following adoptive transfer of CDPs likely reflects a timing issue or a limitation of the transplant model. Finally, analysis of lung and small intestine populations in the BM chimeras confirmed that YFP labeling of CD11b$^+$ cells in all cases results from DNGR-1 expression on BM-derived rather than embryonic precursors (Figures S5C and S5D). This conclusion is further supported by the absence of YFP$^+$ cells in MØ populations from day 14 embryos (data not shown).

Figure 3. *Clec9a*$^{+/cre}$*Rosa*$^{+/EYFP}$ Mice Faithfully Trace CDP-Derived Cells in Spleen and Lymph Node

(A) Live auto$^-$ splenocytes from *Clec9a*$^{+/cre}$*Rosa*$^{+/EYFP}$ mice were gated. YFP expression on CD11c$^+$MHCII$^+$ cells, subset into CD8α$^+$ cDCs (CD8α$^+$CD205$^+$), CD8α$^+$CD205$^-$ pDCs, and CD11b$^+$ DCs, as well as pDCs (SiglecH$^+$B220$^+$). Histogram overlay shows DNGR-1 expression on cDCs.

(B) Percentage of YFP$^+$ cells in the indicated populations.

(C) Immunofluorescence of YFP, CD169, and B220 in spleen from *Clec9a*$^{+/+}$*Rosa*$^{+/EYFP}$ and *Clec9a*$^{+/cre}$*Rosa*$^{+/EYFP}$ mice. Bottom panel is a higher-magnification image of box i.

(D and E) Flow cytometry of sdLN from *Clec9a*$^{+/cre}$*Rosa*$^{+/EYFP}$ mice. (D) YFP expression on CD11c$^+$MHCII^{hi} migrating DCs (CD103$^+$CD207$^+$ and CD103$^-$CD207$^-$ dermal DCs as well as CD103$^-$CD207$^+$ LC). CD11c$^+$MHCII$^+$ resident DCs were subset as in (A). (E) The percentage of YFP$^+$ cells in the indicated populations is shown. (B and E) Each dot represents one mouse. Red indicates high DNGR-1 expression, blue indicates low DNGR-1 expression, and black indicates DNGR-1$^-$ populations. Horizontal bars are the mean from at least two experiments.

See also Figure S3.

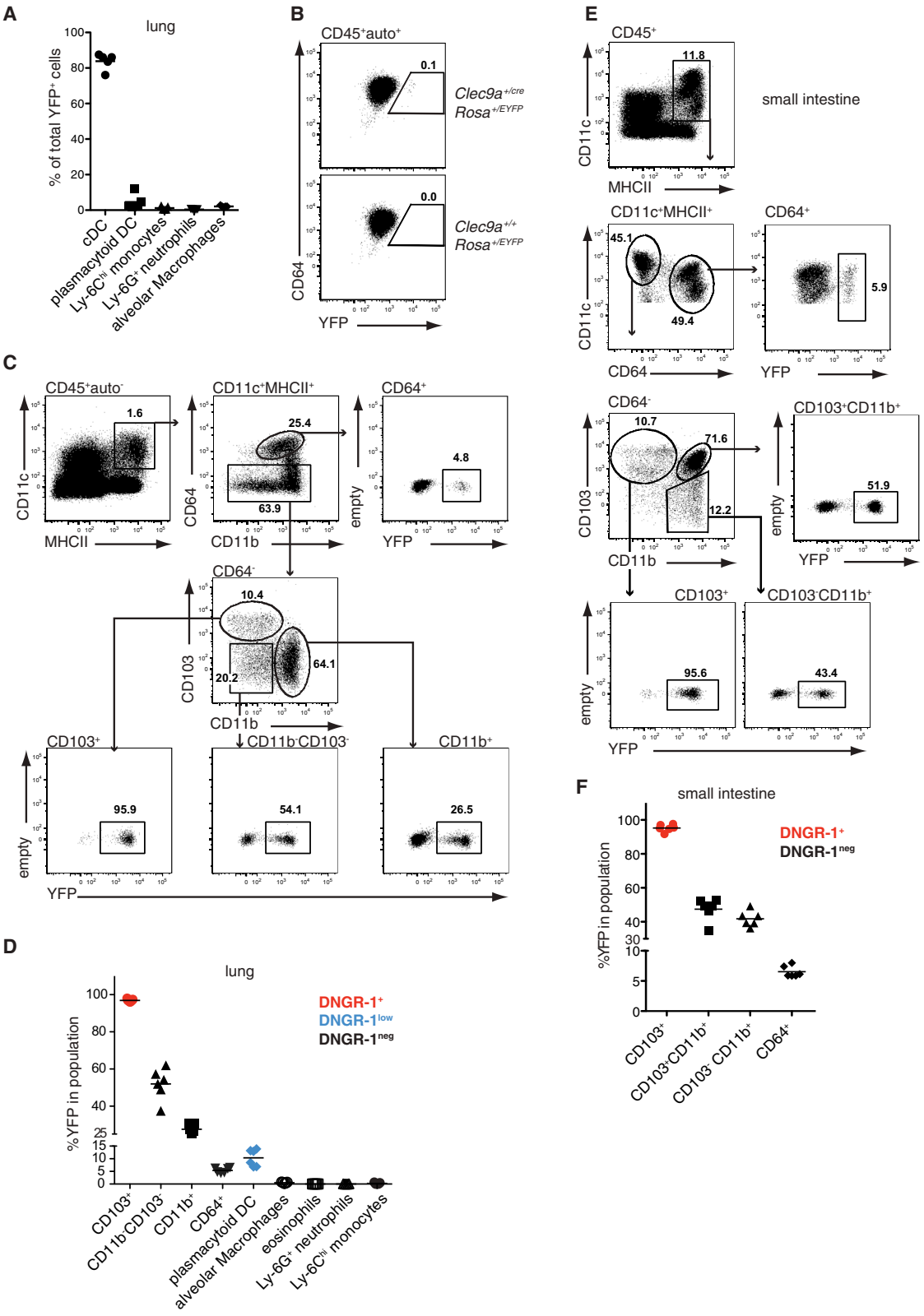

(legend on next page)

Kidney CD64$^+$ CDP-Derived Cells Phenotypically and Functionally Resemble DCs

We next determined whether the unexpected CD64$^+$ CDP progeny in kidney exhibited typical characteristics of cDCs. YFP$^+$ cells were located in the kidney tubular interstitium and showed dendritic morphology with prominent membrane protrusions (Figures 6A and 6B). Most YFP$^+$ cells stained for F4/80 (Figures 6A and 6B), thus corresponding to the CD64$^+$ cells identified by flow cytometry (Figure 5F). We subdivided YFP$^+$ cells into CD64$^+$, CD64$^-$CD11b$^+$, and CD64$^-$CD24$^+$ (i.e., CD11b$^-$) populations. Notably, MHCII expression on CD64$^+$ cells was comparable to that on CD11b$^+$ DCs and was slightly higher than on CD24$^+$ DCs (Figure 6C). When further subdivided, CD64$^+$CD11b^{low}F4/80^{hi} cells expressed higher levels of CD86 than CD64$^+$CD11b^{hi}F4/80^{low} and CD64$^-$CD11b$^+$ DCs but levels comparable to those on CD24$^+$ DCs (Figure 6C). In contrast, CD40 expression was comparable across all kidney DCs.

A hallmark of DCs is the ability to process antigen and to stimulate naive CD4$^+$ T cells. We sorted YFP$^+$CD64$^+$CD11b^{low}F4/80^{hi} cells and cultured them with CFSE-labeled OT-II T cells in the presence or absence of ovalbumin (OVA) protein. As reference antigen-presenting cells (APCs), we included splenic CD11b$^+$ cDCs and B cells. Notably, kidney YFP$^+$CD64$^+$ cells potently stimulated upregulation of CD25 and subsequent proliferation of T cells (Figures 6D and 6E). B cells were inactive in the same assay, whereas splenic CD11b$^+$ cDCs were the most potent APC (Figures 6D and 6E). Both kidney YFP$^+$CD64$^+$ cells and spleen CD11b$^+$ cDCs supported the differentiation of T lymphocytes into effector cells producing interferon-γ (IFN-γ) and tumor necrosis factor-α (TNF-α; Figure 6F). Thus, YFP$^+$CD64$^+$ kidney leukocytes exhibit the morphological, phenotypic, and functional attributes typically associated with cDCs.

Clec9a$^{+/cre}$*Rosa*$^{+/EYFP}$ Mice Faithfully Trace CDP-Derived Cells during Inflammation

Finally, we tested whether *Clec9a*$^{+/cre}$*Rosa*$^{+/EYFP}$ mice can also be used to faithfully trace CDP-derived cells during inflammation, when monocytes differentiate into cells resembling cDCs (Geissmann et al., 2010; Hashimoto et al., 2011; Heath and Carbone, 2009; Steinman and Idoyaga, 2010). Monocytes from *Clec9a*$^{cre/cre}$*Rosa*$^{+/tdRFP}$ mice (similar to *Clec9a*$^{+/cre}$*Rosa*$^{+/EYFP}$ but encoding a variant red fluorescent protein, RFP) were cultured in GM-CSF or GM-CSF + IL-4, conditions that are commonly used to differentiate DC in vitro and are thought to mimic inflammation. Notably, the output of those cultures did not label with RFP despite phenotypically resembling DCs (Figure S6). We then infected *Clec9a*$^{+/cre}$*Rosa*$^{+/EYFP}$ mice with *Listeria monocytogenes*. 24 hr after infection, inflammatory monocyte-derived cells (called "TipDCs" [Serbina et al., 2003b]) could be identified as Gr-1$^+$CD11b^{low} that produce TNF-α (Figure 7A). Importantly, these TipDCs did not label with YFP (Figure 7A), which is in contrast to CD11c$^+$Gr-1$^-$ cDCs (Figure 7B).

It has been shown that monocytes can differentiate into migratory APCs capable of priming naive T cells in models of colitis (Tamoutounour et al., 2012; Zigmond et al., 2012). We therefore analyzed cellular infiltrates in the colon of *Clec9a*$^{+/cre}$*Rosa*$^{+/EYFP}$ mice after 5 days of oral DSS treatment. In colitic colon, DNGR-1 expression remained restricted to CD103$^+$CD11b$^-$ DCs (Figure 7C). We identified monocyte-derived cells as CD11b$^+$ nonneutrophils expressing either Gr-1 or CD64. As reported (Tamoutounour et al., 2012), they encompassed three populations with varying expression levels of MHCII and Gr-1 (Figure 7D; "Mo-waterfall" gate). Importantly, none of these monocyte-derived populations expressed significant levels of YFP (Figure 7D), which is in contrast to CD11c$^+$MHCII$^+$CD64$^-$ cDCs (Figure 7E). Thus, *Clec9a*$^{+/cre}$*Rosa*$^{+/EYFP}$ mice specifically trace CDP, but not monocyte progeny during systemic bacterial infection or acute intestinal inflammation.

DISCUSSION

The classification of mononuclear phagocytes as DCs or MØs is largely based on phenotypic and/or functional criteria. This has led to substantial confusion (Hume, 2008), especially during infection or inflammation when many of the supposedly defining markers and functions of DCs change profoundly (Geissmann et al., 2010; Hashimoto et al., 2011; Heath and Carbone, 2009). The identification of more restricted DC markers has thus far not offered a conclusive resolution to cell type definition. For instance, expression of Zbtb46, which distinguishes cDCs from other lymphoid and myeloid cells, is downregulated after DC stimulation and is additionally found on endothelial cells, early erythroid progenitors, and monocytes stimulated with GM-CSF + IL-4 (Meredith et al., 2012a, 2012b; Satpathy et al., 2012). To circumvent the limitations of an approach based purely on phenotype and function, here we adopt an ontogenetic perspective to define cDCs. We show that DNGR-1 acts as a bona fide marker of mouse cDC precursors and describe a model in which cDCs can be faithfully identified by means of their DNGR-1 expression history. *Clec9a*$^{+/cre}$*Rosa*$^{+/EYFP}$ mice thus provide a genetic model with which to assess the contribution of a committed myeloid precursor to the mononuclear phagocyte system and can be used to define the mouse DC lineage

Figure 4. *Clec9a*$^{+/cre}$*Rosa*$^{+/EYFP}$ Mice Trace CDP-Derived Cells in Lung and Small Intestine

(A–D) Flow cytometry of lung from *Clec9a*$^{+/cre}$*Rosa*$^{+/EYFP}$ mice. (A) Percentage of the indicated populations out of total YFP$^+$ cells. (B) CD64 and YFP expression on CD45$^+$auto$^+$ alveolar MØs. (C) Live CD45$^+$auto$^-$ cells were gated. CD11c$^+$MHCII$^+$ cells were divided into CD64$^+$ and CD64$^-$ cells. Among CD11c$^+$MHCII$^+$ CD64$^-$ cells, *CD103*$^+$*CD11b*$^{-/low}$, *CD103*$^-$*CD11b*$^{-/low}$, and CD103$^-$CD11b$^+$ cells were identified. YFP expression is shown. (D) Percentage of YFP$^+$ cells in the indicated populations is shown.

(E and F) Flow cytometry of small intestine from *Clec9a*$^{+/cre}$*Rosa*$^{+/EYFP}$ mice. (E) Live CD45$^+$ cells were gated. CD11c$^+$MHCII$^+$ cells were divided into *CD64*$^+$*CD11c*$^{+/int}$ and CD64$^-$CD11c^{hi} cells. Among CD64$^-$CD11c^{hi} cells, CD103$^+$CD11b$^-$, CD103$^+$CD11b$^+$, and CD103$^-$CD11b$^+$ cells were identified and analyzed for YFP expression. (F) Percentage of YFP$^+$ cells in the indicated populations.

(D and F) Each dot represents one mouse. Red indicates high DNGR-1 expression, blue indicates low DNGR-1 expression, and black indicates DNGR-1$^-$ populations. Horizontal bars are the mean from two experiments.

See also Figure S4.

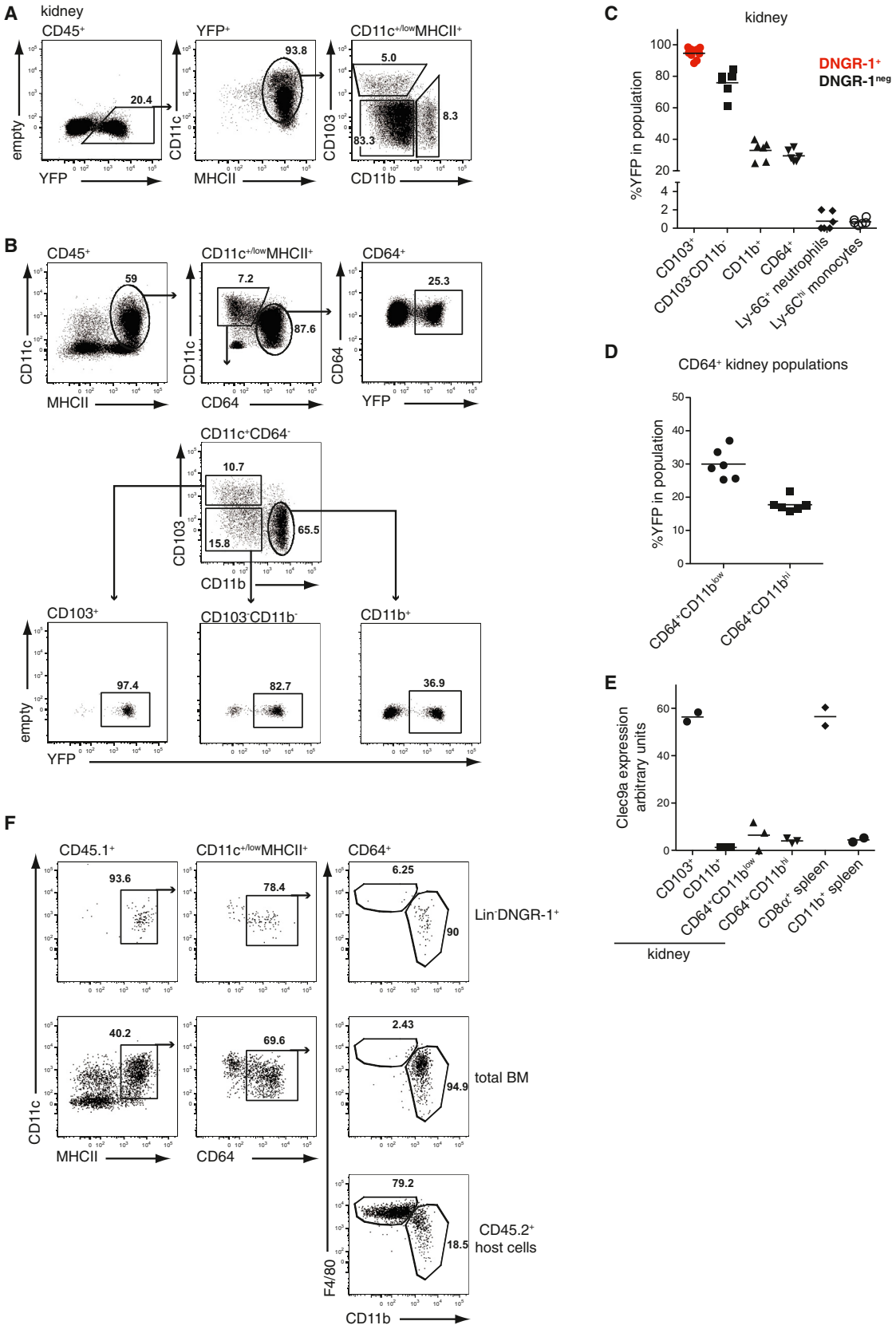

(legend on next page)

from its first committed precursor through to the differentiated state.

DNGR-1$^+$ precursors did not give rise to pDCs in adoptive transfer or genetic labeling experiments, which is consistent with recent suggestions that pDCs arise from a distinct pDC-specific precursor (Cisse et al., 2008; Onai et al., 2013; Satpathy et al., 2012). Such results put in question the existence of a "common DC precursor" that gives rise to cDCs and pDCs, but not monocytes. For simplicity, we continue to refer to the DNGR-1$^+$ precursor as "CDP," although we use this acronym to mean "conventional DC precursor." Intriguingly, CD8α^+CD205$^-$ pDCs, although resembling classical pDCs (Bar-On et al., 2010), were highly labeled with YFP in our reporter mice. Thus, some CD8α^+CD205$^-$ pDCs may arise from CDP, although refined lineage tracing systems, such as a *Clec9a*-driven inducible Cre recombinase, will be needed to fully resolve the issue. Nevertheless, our genetic mapping analysis suggests that similarities in gene expression and transcription factor dependence do not always allow accurate conclusions about cell ontogeny.

Our analysis reveals the presence of CDP-derived cells among the intestinal CD11b$^+$CD103$^-$ mononuclear phagocyte pool, which has previously been suggested to arise from monocytes (Bogunovic et al., 2009; Varol et al., 2009). As those earlier studies did not include the CD64 marker in their analysis, it is conceivable that the monocyte contribution is limited to CD103$^-$CD11b$^+$ cells that express CD64, which likely correspond to CX$_3$CR1^{hi} MØs (Varol et al., 2009). Our fate mapping analysis also reveals the existence of CDP-derived cells within the renal mononuclear CD64$^+$ phagocyte pool. This indicates that CD64 expression does not always mark monocyte progeny and is in line with the emerging concept that mononuclear phagocytes with apparently overlapping phenotype can have distinct origins (Hashimoto et al., 2013; Hoeffel et al., 2012; Schulz et al., 2012). Conversely, our analysis also reveals the presence of cells with distinct phenotypes but common origin such as the ESAM^{hi} and ESAM^{low} spleen cDC populations. Altogether, these observations raise the question of the extent to which nature versus nurture dictates the functions of mononuclear phagocytes. Consistent with a dominant role for nature, YFP$^+$CD64$^+$ kidney cells have morphological, phenotypic, and functional characteristics of cDCs. However, in other circumstances, CDP-derived cells might be poor stimulators of T cells or lack other typical features of DCs. The ability to define DCs on the basis of ontogeny allows for investigation of typical and atypical DC functions and will help to determine the extent to which functions of mononuclear phagocytes are dictated by environmental imprinting.

Due to the incomplete penetrance of labeling, conclusions cannot be drawn about the lack of YFP in any given cell and, instead, YFP needs to be considered at the level of cell populations. We believe the origins of the incomplete labeling lie in the nature of the system rather than in DC heterogeneity. Because of a time lag between Cre protein synthesis and DNA recombination, actively dividing DC precursors (Liu et al., 2009; Onai et al., 2007) can dilute Cre protein before excising the floxed stop cassette. This causes a fraction of the precursors to "escape" labeling in a stochastic fashion, as seen in other fate mapping models (Jakubzick et al., 2008; Ye et al., 2003; Yona et al., 2013). Confirming that notion, increased Cre expression (in homozygous *Clec9a*-Cre mice) leads to markedly increased labeling of DC precursors and near-complete marking of differentiated cDCs (Figure S7). These data confirm that *Clec9a*$^{+/cre}$ *Rosa*$^{+/EYFP}$ mice allow for the identification of CDP-derived populations based on YFP labeling frequencies. The one exception is pDCs, which express low levels of DNGR-1 and in which the presence of YFP is not necessarily an indicator of ontogeny but of receptor expression. Should other cell types upregulate DNGR-1 in specific circumstances, a similar caveat would apply. In such ambiguous cases, YFP analysis may require further refinement, such as the concomitant adoptive transfers presented here.

As shown here, *Clec9a*$^{+/cre}$*Rosa*$^{+/EYFP}$ mice will be especially useful for tracing CDP-derived cells during infection and inflammation. *Clec9a*-Cre mice may also be used to manipulate gene expression specifically in CDP-derived cells, opening perspectives with regards to understanding the functional complexity of the mononuclear phagocyte system. Finally, our data confirm the notion of cDCs as an independent hematopoietic lineage (Naik et al., 2013) and pave the way toward a revised nomenclature of mononuclear phagocytes that takes cell ancestry into account.

EXPERIMENTAL PROCEDURES

Mice

Clec9a$^{+/cre}$, *Clec9a*$^{gfp/gfp}$, Rosa26-stop^{flox}-EYFP (Srinivas et al., 2001), Rosa26-stop^{flox}-tdRFP (Luche et al., 2007), C57BL/6J, and B6.SJL mice were bred at Cancer Research UK in specific pathogen-free conditions. 6- to 10-week-old littermate control mice were used. Animal experiments were performed in accordance with national and institutional guidelines for animal care and approved by the London Research Institute Animal Ethics Committee and by the UK Home Office.

Isolation of Cells

All lymphoid and nonlymphoid tissues, except bone marrow, were subjected to enzymatic digestion with Collagenase IV (200 U/ml; Worthington) and DNase I (0.2 mg/ml, Roche) to isolate cells for flow cytometry.

Figure 5. Lineage Tracing Identifies Previously Unappreciated CDP-Derived Cells in Kidney

(A–D) Flow cytometry of kidney from *Clec9a*$^{+/cre}$*Rosa*$^{+/EYFP}$ mice. (A) Live CD45$^+$ cells were gated. YFP$^+$ cells were analyzed for CD11c, MHCII, CD103, and CD11b expression. (B) CD45$^+$CD11c$^{+/low}$MHCII$^+$ cells were divided into CD64$^+$CD11c^{low} and CD64$^-$CD11c^{hi} cells. Among CD64$^-$CD11c^{hi} cells, CD103$^+$CD11b$^-$, CD103$^-$CD11b$^-$, and CD103$^-$CD11b$^+$ cells were identified and analyzed for YFP expression. (C and D) Percentage of YFP$^+$ cells in the indicated populations (C) and in CD11b^{low} and CD11b^{hi} fractions of CD11c$^{+/low}$MHCII$^+$CD64$^+$ cells (D; see also F). Each dot represents one mouse. Red indicates DNGR-1$^+$ populations, and black indicates DNGR-1$^-$ populations. Horizontal bars are the mean from three experiments.

(E) Clec9a mRNA expression normalized to GapDH in the indicated cell populations as determined by quantitative RT-PCR.

(F) CD45.1$^+$lin$^-$CD115$^+$DNGR-1$^+$ (Figure S1D; n = 5) or total BM cells (n = 6) from B6.SJL mice were transferred i.v. into sublethally irradiated CD45.2 recipients. On day 7, donor-derived kidney cells were analyzed for CD11c, MHCII, and CD64 expression. F4/80 and CD11b expression on CD11c$^{+/low}$MHCII$^+$CD64$^+$ cells was compared to CD45.2$^+$CD64$^+$ host cells.

See also Figure S5.

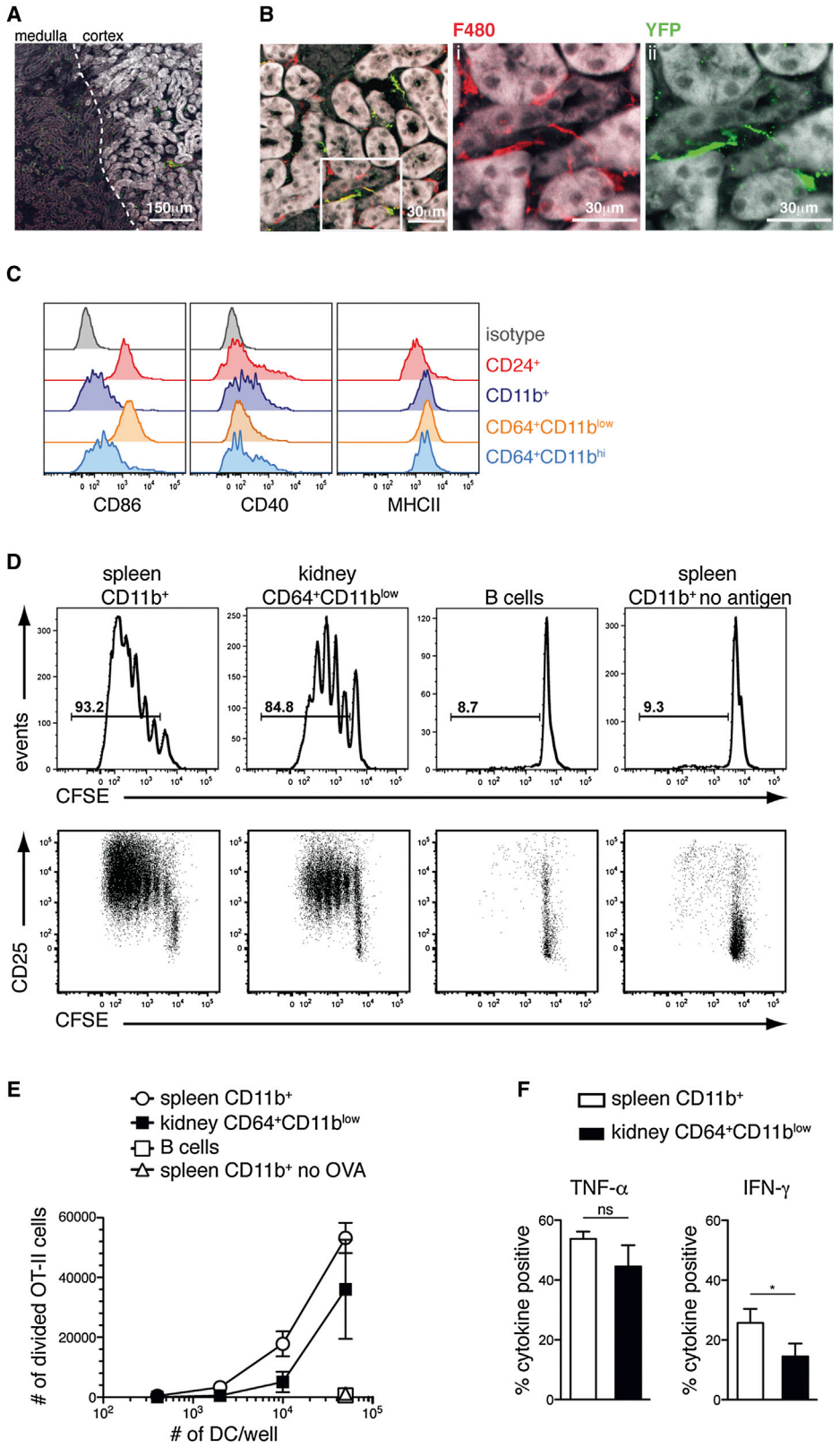

(legend on next page)

Adoptive Transfer

Magnetically enriched lin$^-$ BM cells (Ter119, NK1.1, CD4, CD8, B220, MHCII, CD11b, and CD11c) were stained for CD117, CD115, and DNGR-1 and sorted as lin$^-$CD115$^+$DNGR-1$^+$ cells. 8 × 10^4 lin$^-$CD115$^+$DNGR-1$^+$ or 2 × 10^6 total BM cells were injected intravenously (i.v.) into 3- to 4-week-old unirradiated congenic mice. In some experiments, recipient mice were sublethally irradiated (6.6 Gray) 24 hr before transfer of 6 × 10^4 lin$^-$CD115$^+$DNGR-1$^+$ or 2 × 10^6 total BM cells.

Cell Culture

Carboxyfluorescein succinimidyl ester (CFSE)-labeled OT-II cells (5–10 × 10^4 cells) were cultured with APCs (titrated starting at 5 × 10^4 cells) and OVA protein (10 μg/ml) for 4 days (96 well V-bottom plates). CFSE profiles were analyzed by flow cytometry or cells were restimulated with PMA (10 ng/ml) and ionomycin (1 μg/ml) in the presence of Brefeldin A (5 μg/ml) for 4 hr for intracellular cytokine staining.

2.5 × 10^4 BM monocytes were cultured in complete RPMI supplemented with GM-CSF (10 ng/ml; produced at Cancer Research UK) ± IL-4 (20 ng/ml; R&D systems) for 5 days. On day 3, half of the media was replaced with fresh cytokine cocktail.

Image Stream

Samples were acquired on a 4-laser, six channel ISx imaging flow cytometer at 60× magnification and analyzed using IDEAS 5.0 (both IFC, Amnis). At least 1 × 10^5 single cells were collected using a bright-field threshold. A compensation matrix was generated using single-color controls to perform postacquisition spectral correction on a per pixel, per channel basis (Filby and Davies, 2012).

Microscopy

Mice were perfused with 2% paraformaldehyde (PFA)/PBS, tissues harvested and fixed in 2% PFA/PBS for 24 hr, then incubated in 30% sucrose/H_2O overnight and frozen in OCT. 10 μm sections were air-dried, fixed (4%PFA, 10 min), washed in PBS, permeabilized (0.2% TritonX/PBS), blocked with PBS/10% rabbit serum, 1% BSA, 0.1% Tween20 (30 min), and stained in PBS 1% BSA, 0.1% Tween20 (1–2 hr) at room temperature. Confocal microscopy was done on a Zeiss 710 upright microscope with 20× and 10× objectives and analyzed with ImageJ and Bitplane Imaris software.

Mixed BM Chimeras

24 hr after irradiation (two doses of 6.6 Gray separated by 4 hr), CD45.2$^+$ C57BL/6J mice were injected i.v. with 2 × 10^6 total BM cells at a 1:1 mixture of CD45.1 B6.SJL to CD45.2 *Clec9a*$^{+/cre}$*Rosa*$^{+/EYFP}$ or CD45.1 B6.SJL to CD45.2 *Clec9a*$^{+/+}$*Rosa*$^{+/EYFP}$ BM. Mice were analyzed 6–8 weeks after reconstitution.

Infections

Mice were infected i.v. with 5,000 CFU recombinant *Listeria monocytogenes*-OVA (LM-OVA, kindly provided by Leo Lefrançois). 24 hr later, splenocytes were isolated by collagenase digestion and cultured in complete RPMI with Brefeldin A for 4 hr, with or without heat-killed LM-OVA (HKLM, prepared by incubation at 70°C for 3 hr [Lauvau et al., 2001]) added at a 50:1 ratio of HKLM:splenocytes (Serbina et al., 2003a).

DSS Colitis

Mice received Dextran Sulfate Sodium Salt (DSS, 2%) in drinking water as described (Wirtz et al., 2007; Zigmond et al., 2012) and were monitored for weight loss every day. On day 5 of DSS treatment, colons were analyzed.

SUPPLEMENTAL INFORMATION

Supplemental Information includes Extended Experimental Procedures and seven figures and can be found with this article online at http://dx.doi.org/10.1016/j.cell.2013.07.014.

ACKNOWLEDGMENTS

We thank Frederic Geissmann and members of the Immunobiology Laboratory for helpful discussions and suggestions. C.R.S. is funded by Cancer Research UK, a prize from Fondation Bettencourt-Schueller, and a grant from the European Research Council (ERC Advanced Researcher Grant AdG-2010-268670). B.U.S. was supported by an EMBO long-term fellowship, J.v.B. was supported by Boehringer Ingelheim Fonds, P.G.W. was supported by an Overseas Biomedical Fellowship from the NHMRC of Australia, and S.E.A. was supported by a Henry Wellcome Fellowship (WT089009MA). We thank CRUK Transgenic Services for generation of genetically modified mice and the Biological Resources staff for animal care and assistance with mouse experiments. We thank Yasmine Belkaid and John Grainger for their help with the isolation of intestinal lamina propria cells.

Received: December 19, 2012
Revised: May 2, 2013
Accepted: July 11, 2013
Published: August 15, 2013

REFERENCES

Auffray, C., Fogg, D.K., Narni-Mancinelli, E., Senechal, B., Trouillet, C., Saederup, N., Leemput, J., Bigot, K., Campisi, L., Abitbol, M., et al. (2009). CX3CR1+ CD115+ CD135+ common macrophage/DC precursors and the role of CX3CR1 in their response to inflammation. J. Exp. Med. *206*, 595–606.

Bar-On, L., Birnberg, T., Lewis, K.L., Edelson, B.T., Bruder, D., Hildner, K., Buer, J., Murphy, K.M., Reizis, B., and Jung, S. (2010). CX3CR1+ CD8alpha+ dendritic cells are a steady-state population related to plasmacytoid dendritic cells. Proc. Natl. Acad. Sci. USA *107*, 14745–14750.

Bogunovic, M., Ginhoux, F., Helft, J., Shang, L., Hashimoto, D., Greter, M., Liu, K., Jakubzick, C., Ingersoll, M.A., Leboeuf, M., et al. (2009). Origin of the lamina propria dendritic cell network. Immunity *31*, 513–525.

Caminschi, I., Proietto, A.I., Ahmet, F., Kitsoulis, S., Shin Teh, J., Lo, J.C.Y., Rizzitelli, A., Wu, L., Vremec, D., van Dommelen, S.L.H., et al. (2008). The dendritic cell subtype-restricted C-type lectin Clec9A is a target for vaccine enhancement. Blood *112*, 3264–3273.

Chorro, L., Sarde, A., Li, M., Woollard, K.J., Chambon, P., Malissen, B., Kissenpfennig, A., Barbaroux, J.B., Groves, R., and Geissmann, F. (2009). Langerhans cell (LC) proliferation mediates neonatal development, homeostasis, and inflammation-associated expansion of the epidermal LC network. J. Exp. Med. *206*, 3089–3100.

Cisse, B., Caton, M.L., Lehner, M., Maeda, T., Scheu, S., Locksley, R., Holmberg, D., Zweier, C., den Hollander, N.S., Kant, S.G., et al. (2008). Transcription factor E2-2 is an essential and specific regulator of plasmacytoid dendritic cell development. Cell *135*, 37–48.

Desch, A.N., Randolph, G.J., Murphy, K., Gautier, E.L., Kedl, R.M., Lahoud, M.H., Caminschi, I., Shortman, K., Henson, P.M., and Jakubzick, C.V.

Figure 6. Kidney CD64$^+$ CDP-Derived Cells Exhibit Phenotypic and Functional Properties of cDCs

(A and B) Immunofluorescence of kidney from *Clec9a*$^{+/cre}$*Rosa*$^{+/EYFP}$ mice stained for F4/80 (red) and YFP (green). Grayscale (autofluorescence) shows kidney architecture. Dotted line shows divide between cortex and medulla. (B) Renal cortex. Panels i (F4/80) and ii (YFP) are higher-magnification images of the box inset.
(C) Expression of CD86, CD40, and MHCII on YFP$^+$ kidney leukocytes subset into CD64$^+$CD11c^{low} and CD64$^-$CD11c^{hi} cells as in Figure 5B. CD24 identifies CD64$^-$CD103$^+$CD11b$^-$ and CD64$^-$CD103$^-$CD11b$^-$ cells (not shown).
(D–F) CFSE-labeled OT-II T cells were cultured with sorted splenic CD11b$^+$ DCs, B cells, or kidney YFP$^+$CD64$^+$CD11b^{low} cells and OVA for 4 days. (D) CFSE dilution profiles and CD25 expression on OT-II cells cultured with 5 × 10^4 APC. (E) The number of divided OT-II cells per well, assessed by CFSE dilution. (F) On day 4, OT-II T cells cultured with 5 × 10^4 APC were restimulated with PMA/ionomycin. Percentage of IFN-γ and TNF-α producing OT-II cells was determined by intracellular staining. (E and F) Mean ± SD; n = 3, representative of three experiments; *$p < 0.05$; ns, not significant; unpaired Student's t test.

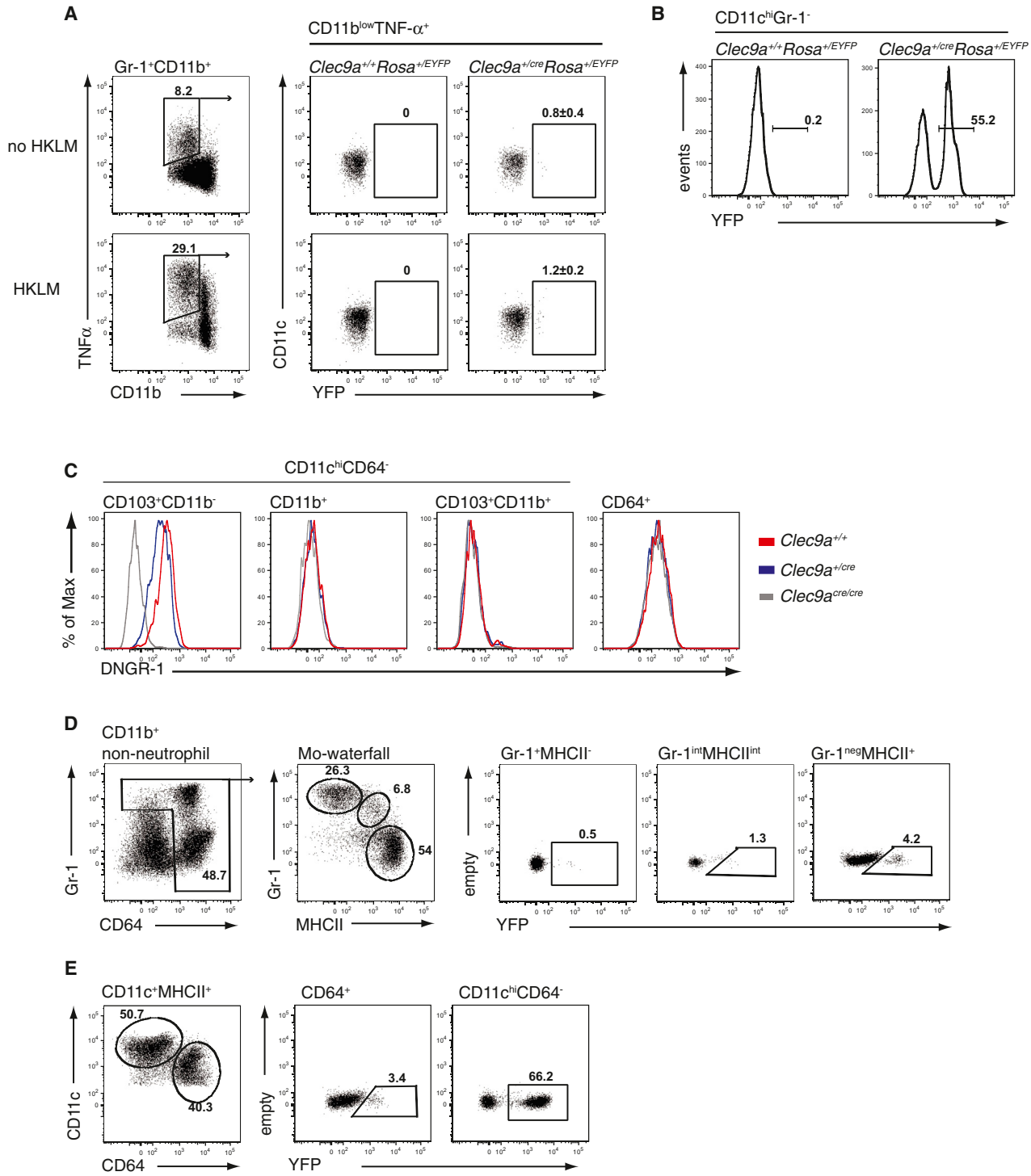

Figure 7. *Clec9a*$^{+/cre}$*Rosa*$^{+/EYFP}$ Mice Trace CDP-Derived Cells in Inflammation

(A and B) Splenocytes from *L. monocytogenes*-infected *Clec9a*$^{+/+}$*Rosa*$^{+/EYFP}$ and *Clec9a*$^{+/cre}$*Rosa*$^{+/EYFP}$ mice, untreated or restimulated with heat-killed *L. monocytogenes* (HKLM). YFP expression in Gr-1$^+$CD11b^{low}TNF-α$^+$ TipDCs (A) (mean ± SD, n = 5) and CD11c$^+$Gr-1$^-$ cells (B) is shown.

(C–E) Flow cytometry of colitic colons from *Clec9a*$^{+/+}$*Rosa*$^{+/EYFP}$, *Clec9a*$^{+/cre}$*Rosa*$^{+/EYFP}$, and *Clec9a*$^{cre/cre}$*Rosa*$^{+/EYFP}$ mice after 5 days of DSS treatment. (C) DNGR-1 expression on CD11c$^+$MHCII$^+$ cells, divided into CD64$^+$ and CD64$^-$CD11c^{hi} cells (CD103$^+$CD11b$^-$, CD103$^+$CD11b$^+$, and CD103$^-$CD11b$^+$; see Figure 4E). (D) YFP expression on monocyte-derived cells from *Clec9a*$^{+/cre}$*Rosa*$^{+/EYFP}$ mice identified as CD11b$^+$ nonneutrophils expressing Gr-1 or CD64 (Tamoutounour et al., 2012; Mo-waterfall) and further divided into Gr-1$^+$MHCII^{neg}, CD11c^{int}MHCII^{int}, and Gr-1^{neg}MHCII$^+$ cells. (E) YFP expression in CD64$^+$ and CD64$^-$ CD11c$^+$MHCII$^+$ cells from *Clec9a*$^{+/cre}$*Rosa*$^{+/EYFP}$ mice.

(2011). CD103+ pulmonary dendritic cells preferentially acquire and present apoptotic cell-associated antigen. J. Exp. Med. *208*, 1789–1797.

Edelson, B.T., Kc, W., Juang, R., Kohyama, M., Benoit, L.A., Klekotka, P.A., Moon, C., Albring, J.C., Ise, W., Michael, D.G., et al. (2010). Peripheral CD103+ dendritic cells form a unified subset developmentally related to CD8alpha+ conventional dendritic cells. J. Exp. Med. *207*, 823–836.

Filby, A., and Davies, D. (2012). Reporting imaging flow cytometry data for publication: why mask the detail? Cytometry A *81*, 637–642.

Fogg, D.K., Sibon, C., Miled, C., Jung, S., Aucouturier, P., Littman, D.R., Cumano, A., and Geissmann, F. (2006). A clonogenic bone marrow progenitor specific for macrophages and dendritic cells. Science *311*, 83–87.

Gautier, E.L., Shay, T., Miller, J., Greter, M., Jakubzick, C., Ivanov, S., Helft, J., Chow, A., Elpek, K.G., Gordonov, S., et al.; Immunological Genome Consortium. (2012). Gene-expression profiles and transcriptional regulatory pathways that underlie the identity and diversity of mouse tissue macrophages. Nat. Immunol. *13*, 1118–1128.

Geissmann, F., Manz, M.G., Jung, S., Sieweke, M.H., Merad, M., and Ley, K. (2010). Development of monocytes, macrophages, and dendritic cells. Science *327*, 656–661.

Ginhoux, F., Liu, K., Helft, J., Bogunovic, M., Greter, M., Hashimoto, D., Price, J., Yin, N., Bromberg, J., Lira, S.A., et al. (2009). The origin and development of nonlymphoid tissue CD103+ DCs. J. Exp. Med. *206*, 3115–3130.

Greter, M., Helft, J., Chow, A., Hashimoto, D., Mortha, A., Agudo-Cantero, J., Bogunovic, M., Gautier, E.L., Miller, J., Leboeuf, M., et al. (2012). GM-CSF controls nonlymphoid tissue dendritic cell homeostasis but is dispensable for the differentiation of inflammatory dendritic cells. Immunity *36*, 1031–1046.

Haniffa, M., Shin, A., Bigley, V., McGovern, N., Teo, P., See, P., Wasan, P.S., Wang, X.N., Malinarich, F., Malleret, B., et al. (2012). Human tissues contain CD141hi cross-presenting dendritic cells with functional homology to mouse CD103+ nonlymphoid dendritic cells. Immunity *37*, 60–73.

Hashimoto, D., Miller, J., and Merad, M. (2011). Dendritic cell and macrophage heterogeneity in vivo. Immunity *35*, 323–335.

Hashimoto, D., Chow, A., Noizat, C., Teo, P., Beasley, M.B., Leboeuf, M., Becker, C.D., See, P., Price, J., Lucas, D., et al. (2013). Tissue-resident macrophages self-maintain locally throughout adult life with minimal contribution from circulating monocytes. Immunity *38*, 792–804.

Heath, W.R., and Carbone, F.R. (2009). Dendritic cell subsets in primary and secondary T cell responses at body surfaces. Nat. Immunol. *10*, 1237–1244.

Hildner, K., Edelson, B.T., Purtha, W.E., Diamond, M., Matsushita, H., Kohyama, M., Calderon, B., Schraml, B.U., Unanue, E.R., Diamond, M.S., et al. (2008). Batf3 deficiency reveals a critical role for CD8alpha+ dendritic cells in cytotoxic T cell immunity. Science *322*, 1097–1100.

Hoeffel, G., Wang, Y., Greter, M., See, P., Teo, P., Malleret, B., Leboeuf, M., Low, D., Oller, G., Almeida, F., et al. (2012). Adult Langerhans cells derive predominantly from embryonic fetal liver monocytes with a minor contribution of yolk sac-derived macrophages. J. Exp. Med. *209*, 1167–1181.

Hume, D.A. (2008). Macrophages as APC and the dendritic cell myth. J. Immunol. *181*, 5829–5835.

Jakubzick, C., Bogunovic, M., Bonito, A.J., Kuan, E.L., Merad, M., and Randolph, G.J. (2008). Lymph-migrating, tissue-derived dendritic cells are minor constituents within steady-state lymph nodes. J. Exp. Med. *205*, 2839–2850.

Langlet, C., Tamoutounour, S., Henri, S., Luche, H., Ardouin, L., Grégoire, C., Malissen, B., and Guilliams, M. (2012). CD64 expression distinguishes monocyte-derived and conventional dendritic cells and reveals their distinct role during intramuscular immunization. J. Immunol. *188*, 1751–1760.

Lauvau, G., Vijh, S., Kong, P., Horng, T., Kerksiek, K., Serbina, N., Tuma, R.A., and Pamer, E.G. (2001). Priming of memory but not effector CD8 T cells by a killed bacterial vaccine. Science *294*, 1735–1739.

Lewis, K.L., Caton, M.L., Bogunovic, M., Greter, M., Grajkowska, L.T., Ng, D., Klinakis, A., Charo, I.F., Jung, S., Gommerman, J.L., et al. (2011). Notch2 receptor signaling controls functional differentiation of dendritic cells in the spleen and intestine. Immunity *35*, 780–791.

Liu, K., Victora, G.D., Schwickert, T.A., Guermonprez, P., Meredith, M.M., Yao, K., Chu, F.-F., Randolph, G.J., Rudensky, A.Y., and Nussenzweig, M. (2009). In vivo analysis of dendritic cell development and homeostasis. Science *324*, 392–397.

Luche, H., Weber, O., Nageswara Rao, T., Blum, C., and Fehling, H.J. (2007). Faithful activation of an extra-bright red fluorescent protein in "knock-in" Cre-reporter mice ideally suited for lineage tracing studies. Eur. J. Immunol. *37*, 43–53.

Meredith, M.M., Liu, K., Darrasse-Jeze, G., Kamphorst, A.O., Schreiber, H.A., Guermonprez, P., Idoyaga, J., Cheong, C., Yao, K.H., Niec, R.E., and Nussenzweig, M.C. (2012a). Expression of the zinc finger transcription factor zDC (Zbtb46, Btbd4) defines the classical dendritic cell lineage. J. Exp. Med. *209*, 1153–1165.

Meredith, M.M., Liu, K., Kamphorst, A.O., Idoyaga, J., Yamane, A., Guermonprez, P., Rihn, S., Yao, K.H., Silva, I.T., Oliveira, T.Y., et al. (2012b). Zinc finger transcription factor zDC is a negative regulator required to prevent activation of classical dendritic cells in the steady state. J. Exp. Med. *209*, 1583–1593.

Miller, J.C., Brown, B.D., Shay, T., Gautier, E.L., Jojic, V., Cohain, A., Pandey, G., Leboeuf, M., Elpek, K.G., Helft, J., et al.; Immunological Genome Consortium. (2012). Deciphering the transcriptional network of the dendritic cell lineage. Nat. Immunol. *13*, 888–899.

Milling, S., Yrlid, U., Cerovic, V., and MacPherson, G. (2010). Subsets of migrating intestinal dendritic cells. Immunol. Rev. *234*, 259–267.

Naik, S.H., Metcalf, D., van Nieuwenhuijze, A., Wicks, I., Wu, L., O'Keeffe, M., and Shortman, K. (2006). Intrasplenic steady-state dendritic cell precursors that are distinct from monocytes. Nat. Immunol. *7*, 663–671.

Naik, S.H., Sathe, P., Park, H.-Y., Metcalf, D., Proietto, A.I., Dakic, A., Carotta, S., O'Keeffe, M., Bahlo, M., Papenfuss, A., et al. (2007). Development of plasmacytoid and conventional dendritic cell subtypes from single precursor cells derived in vitro and in vivo. Nat. Immunol. *8*, 1217–1226.

Naik, S.H., Perié, L., Swart, E., Gerlach, C., van Rooij, N., de Boer, R.J., and Schumacher, T.N. (2013). Diverse and heritable lineage imprinting of early haematopoietic progenitors. Nature *496*, 229–232.

Onai, N., Obata-Onai, A., Schmid, M.A., Ohteki, T., Jarrossay, D., and Manz, M.G. (2007). Identification of clonogenic common Flt3+M-CSFR+ plasmacytoid and conventional dendritic cell progenitors in mouse bone marrow. Nat. Immunol. *8*, 1207–1216.

Onai, N., Kurabayashi, K., Hosoi-Amaike, M., Toyama-Sorimachi, N., Matsushima, K., Inaba, K., and Ohteki, T. (2013). A clonogenic progenitor with prominent plasmacytoid dendritic cell developmental potential. Immunity *38*, 943–957.

Persson, E.K., Uronen-Hansson, H., Semmrich, M., Rivollier, A., Hägerbrand, K., Marsal, J., Gudjonsson, S., Håkansson, U., Reizis, B., Kotarsky, K., and Agace, W.W. (2013). IRF4 transcription-factor-dependent CD103(+) CD11b(+) dendritic cells drive mucosal T helper 17 cell differentiation. Immunity *38*, 958–969.

Plantinga, M., Guilliams, M., Vanheerswynghels, M., Deswarte, K., Branco-Madeira, F., Toussaint, W., Vanhoutte, L., Neyt, K., Killeen, N., Malissen, B., et al. (2013). Conventional and monocyte-derived CD11b(+) dendritic cells initiate and maintain T helper 2 cell-mediated immunity to house dust mite allergen. Immunity *38*, 322–335.

Poulin, L.F., Reyal, Y., Uronen-Hansson, H., Schraml, B.U., Sancho, D., Murphy, K.M., Håkansson, U.K., Moita, L.F., Agace, W.W., Bonnet, D., and Reis e Sousa, C. (2012). DNGR-1 is a specific and universal marker of mouse and human Batf3-dependent dendritic cells in lymphoid and nonlymphoid tissues. Blood *119*, 6052–6062.

Sancho, D., Mourão-Sá, D., Joffre, O.P., Schulz, O., Rogers, N.C., Pennington, D.J., Carlyle, J.R., and Reis e Sousa, C. (2008). Tumor therapy in mice via antigen targeting to a novel, DC-restricted C-type lectin. J. Clin. Invest. *118*, 2098–2110.

Sancho, D., Joffre, O.P., Keller, A.M., Rogers, N.C., Martínez, D., Hernanz-Falcón, P., Rosewell, I., and Reis e Sousa, C. (2009). Identification of a dendritic

cell receptor that couples sensing of necrosis to immunity. Nature *458*, 899–903.

Satpathy, A.T., Murphy, K.M., and Kc, W. (2011). Transcription factor networks in dendritic cell development. Semin. Immunol. *23*, 388–397.

Satpathy, A.T., Kc, W., Albring, J.C., Edelson, B.T., Kretzer, N.M., Bhattacharya, D., Murphy, T.L., and Murphy, K.M. (2012). Zbtb46 expression distinguishes classical dendritic cells and their committed progenitors from other immune lineages. J. Exp. Med. *209*, 1135–1152.

Schlenner, S.M., Madan, V., Busch, K., Tietz, A., Läufle, C., Costa, C., Blum, C., Fehling, H.J., and Rodewald, H.-R. (2010). Fate mapping reveals separate origins of T cells and myeloid lineages in the thymus. Immunity *32*, 426–436.

Schlitzer, A., McGovern, N., Teo, P., Zelante, T., Atarashi, K., Low, D., Ho, A.W., See, P., Shin, A., Wasan, P.S., et al. (2013). IRF4 transcription factor-dependent CD11b+ dendritic cells in human and mouse control mucosal IL-17 cytokine responses. Immunity *38*, 970–983.

Schulz, C., Gomez Perdiguero, E., Chorro, L., Szabo-Rogers, H., Cagnard, N., Kierdorf, K., Prinz, M., Wu, B., Jacobsen, S.E.W., Pollard, J.W., et al. (2012). A lineage of myeloid cells independent of Myb and hematopoietic stem cells. Science *336*, 86–90.

Serbina, N.V., Kuziel, W., Flavell, R., Akira, S., Rollins, B., and Pamer, E.G. (2003a). Sequential MyD88-independent and -dependent activation of innate immune responses to intracellular bacterial infection. Immunity *19*, 891–901.

Serbina, N.V., Salazar-Mather, T.P., Biron, C.A., Kuziel, W.A., and Pamer, E.G. (2003b). TNF/iNOS-producing dendritic cells mediate innate immune defense against bacterial infection. Immunity *19*, 59–70.

Srinivas, S., Watanabe, T., Lin, C.S., William, C.M., Tanabe, Y., Jessell, T.M., and Costantini, F. (2001). Cre reporter strains produced by targeted insertion of EYFP and ECFP into the ROSA26 locus. BMC Dev. Biol. *1*, 4.

Steinman, R.M., and Idoyaga, J. (2010). Features of the dendritic cell lineage. Immunol. Rev. *234*, 5–17.

Tamoutounour, S., Henri, S., Lelouard, H., de Bovis, B., de Haar, C., van der Woude, C.J., Woltman, A.M., Reyal, Y., Bonnet, D., Sichien, D., et al. (2012). CD64 distinguishes macrophages from dendritic cells in the gut and reveals the Th1-inducing role of mesenteric lymph node macrophages during colitis. Eur. J. Immunol. *42*, 3150–3166.

Tussiwand, R., Lee, W.L., Murphy, T.L., Mashayekhi, M., Wumesh, K.C., Albring, J.C., Satpathy, A.T., Rotondo, J.A., Edelson, B.T., Kretzer, N.M., et al. (2012). Compensatory dendritic cell development mediated by BATF-IRF interactions. Nature *490*, 502–507.

Varol, C., Vallon-Eberhard, A., Elinav, E., Aychek, T., Shapira, Y., Luche, H., Fehling, H.J., Hardt, W.-D., Shakhar, G., and Jung, S. (2009). Intestinal lamina propria dendritic cell subsets have different origin and functions. Immunity *31*, 502–512.

Wirtz, S., Neufert, C., Weigmann, B., and Neurath, M.F. (2007). Chemically induced mouse models of intestinal inflammation. Nat. Protoc. *2*, 541–546.

Ye, M., Iwasaki, H., Laiosa, C.V., Stadtfeld, M., Xie, H., Heck, S., Clausen, B., Akashi, K., and Graf, T. (2003). Hematopoietic stem cells expressing the myeloid lysozyme gene retain long-term, multilineage repopulation potential. Immunity *19*, 689–699.

Yona, S., Kim, K.W., Wolf, Y., Mildner, A., Varol, D., Breker, M., Strauss-Ayali, D., Viukov, S., Guilliams, M., Misharin, A., et al. (2013). Fate mapping reveals origins and dynamics of monocytes and tissue macrophages under homeostasis. Immunity *38*, 79–91.

Zigmond, E., Varol, C., Farache, J., Elmaliah, E., Satpathy, A.T., Friedlander, G., Mack, M., Shpigel, N., Boneca, I.G., Murphy, K.M., et al. (2012). Ly6C hi monocytes in the inflamed colon give rise to proinflammatory effector cells and migratory antigen-presenting cells. Immunity *37*, 1076–1090.